Automatic Reconstruction of Road Centerlines from Mobile Mapping Image Sequences

Chuang Tao, Rongxing Li, and Michael A. Chapman

Abstract

An automatic approach to road centerline reconstruction from stereo image sequences acquired by a mobile mapping system is introduced. The road centerline reconstruction is treated as an inverse problem and solved by global optimization techniques. The centerlines are described by a physical curve model, which is composed of an abstract material and deforms according to external and internal forces applied. The external forces, generated from the centerline information extracted from the image sequences, controls the local characteristics of the model. The internal forces, arising from a priori *knowledge of the road shape, contribute to the global shape of the model. Unique constraints that exist only in mobile mapping image sequences are utilized. The developed system has been used for processing a large number of mobile mapping image sequences. Road centerlines of the images under different conditions have been reconstructed successfully. The research results also make a contribution to the general field of structure from motion and stereo.*

Introduction

Transportation related applications such as road surface inspection and maintenance, fleet management, and automatic vehicle navigation require high quality and up-to-date road network databases. Road centerline information is a fundamental component of the databases. Based on the road centerlines, important indicators of road maintenance, such as dynamic segments, longitudinal profiles, and road surface deformation parameters, can be defined and managed. The acquisition of up-to-date road centerlines using conventional field surveying methods is a time consuming and costly task. Since 1992, a mobile mapping system, VISAT™, has been under development by The University of Calgary and GEOFIT Inc., Laval, Quebec for rapid highway spatial data collection (Schwarz *et al.*, 1993; Li *et al.*, 1994). In this system, CCD (charge coupled device) cameras mounted on the top of a moving van collect stereoscopic image sequences of objects along the road. The image sequences are georeferenced using data from integrated GPS (Global Positioning System) and INS (inertial navigation system) sensors. That implies that orientation parameters of the images are available. The information about road centerlines is extracted from the image sequences by a post-mission processing. Their positions in the scene domain can be calculated by photogrammetric triangulation. A challenging issue in this processing procedure is the automation of centerline extraction from the vast amount of the captured image data.

Research on automatic extraction of road centerline information from imagery for autonomous vehicle navigation has been conducted by Dickmann and Zapp (1986), Thorpe *et al.* (1988), Dickinson and Davis (1990), and Schneiderman and Nashman (1994). The outcome of the research indicated that the automatic extraction of road centerline information using imagery alone seems to give a partial solution due to the limited information from images and the complexity of road conditions. Examples of situations where the automation process can be affected include (1) centerlines with missing, intermittent, or faded markings; (2) variation of making types, especially those of lane makings, and disturbance by other marking categories such as stop lines and direction arrows; (3) lighting conditions (for example, sunshine, rain, cloudiness, or shadowing by trees, buildings, and other objects); (4) road surface materials such as concrete or asphalt and road conditions such as snow covered or wet; and (5) road shapes, for example, straight or curved road segments, and intersections. Because of the perspective nature of the images, there are great scale variations within the images. Furthermore, occlusions, for example, by moving vehicles might occur. Figure 1 illustrates three examples of images captured by the mobile mapping system. Methods for object identification from image sequences (Geiselmann and Hahn, 1994a; Geiselmann and Hahn, 1994b) are not specifically dealt with. To simplify the description in the following sections without losing generality, road centers and lane separating lines are all referred to as centerlines.

He and Novak (1992) initiated automatic centerline information extraction using mobile mapping data. In the present research, the reconstruction of 3D objects from mobile mapping data is treated as an ill-posed vision problem (Jolion, 1994) and solved by adding constraints derived from integrated sensors of the mobile mapping system such as GPS, INS, and CCD cameras. These constraints are unique, and prove to be efficient for road information extraction and reconstruction.

This paper introduces an integrated approach to automatic road centerline reconstruction from mobile mapping image sequences. An approximate 3D road centerline profile model is set at the beginning (Figure 2). Because the navigation data provide the transformation between the approximate model and the stereoscopic image sequences, approximate 2D centerlines in the images can be predicted. Differences between the approximate centerlines and detected centerlines in the image sequences are used to update and refine the model in the scene domain. This procedure is described by an inverse problem and solved using global dynamic energy

C. Tao and M.A. Chapman are with the Department of Geomatics Engineering, The University of Calgary, Calgary, Alberta T2N 1N4, Canada.

R. Li is with the Department of Civil and Environmental Engineering and Geodetic Science, The Ohio State University, Columbus, OH 43210 (li.282@osu.edu).

Photogrammetric Engineering & Remote Sensing, Vol. 64, No. 7, July 1998, pp. 709–716.

0099-1112/98/6407–709$3.00/0
© 1998 American Society for Photogrammetry and Remote Sensing

(a) (b) (c)

Figure 1. Examples of road centerlines from the image sequences: (a) pedestrian crossing creating a large gap along a lane separating line, (b) shadow of a building changing image contrast and a car blocking a portion of the line, and (c) curved lines at a T-intersection.

minimization. A detailed diagram of this approach is illustrated in Figure 3.

First, a 3D approximate road centerline model with one line on each side of the vehicle is calculated by means of a B-spline function using the vehicle trajectory derived from kinematic GPS/INS data. This approximate model assumes that the vehicle is usually driven close to the middle of a lane that has a constant known lane width. Second, this 3D model is projected back onto the stereoscopic image sequences through known orientation parameters of the cameras. The specific line on one side of the vehicle to be extracted is identified by a mouse-click on the image screen. In the image domain, a geometric and photometric model of the road centerlines is established. This image domain model is used to guide the extraction of road centerline feature points in the images, considering the projected road centerlines. Third, a stereo matching algorithm determines a set of stereo pairs of matched centerline feature points considering stereo and image sequence constraints. After a photogrammetric triangulation, the matched feature points are transformed to 3D feature points of the road centerlines in the scene domain. Next, the centerline model is defined as an active deformable 3D curve (3D snake) with a physical deformation model. This model deforms progressively, driven by internal and external energies. The internal energy arises from constraints representing natural characteristics of the centerline shape, such as smoothness. It enforces the estimated centerline to maintain the shape defined by *a priori* knowledge about the centerline shape. The matched 3D feature points act as the external energy and lead the model to deform towards their positions. The interaction between the internal and external forces balances the model, which is deformed incrementally towards the final state. An iterative procedure is needed to update the approximate model by using successive image pairs. Finally, after the iterations are complete, the deformation curve is treated as an optimal 3D road centerline model.

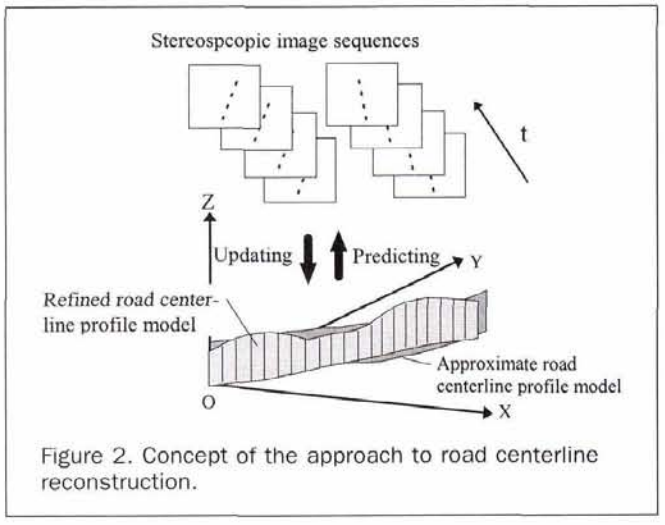

Figure 2. Concept of the approach to road centerline reconstruction.

The following sections describe the details of the approach, including generation of the approximate 3D centerline model, extraction of centerline information from image sequences, and dynamic refinement of the 3D physical centerline model. Results of implementation and evaluation of the approach are also presented.

Generation of an Approximate Road Centerline Model

Generation of an approximate 3D centerline is a key step to start the overall procedure. The 3D vehicle trajectory is determined by GPS/INS components (Schwarz *et al.*, 1993) and is used to derive the approximate model. A 3D cubic B-spline function defines the shape of a centerline as a vector state of points along the curve: i.e.,

$$Q(u_j) = (x(u_j), y(u_j), z(u_j)) = \sum_{i=0}^{m-1} V_i B_i(u_j), \quad j=0,1,\ldots,n-1 \qquad (1)$$

where B_i is the ith basis function of the B-spline, $V_i=(X_i,Y_i,Z_i)$ are the coordinates of the ith control vertex of the curve, n is the number of sampling points along the curve, and m is the number of control vertices. The B-spline is chosen to represent the centerline model based on its following characteristics:

- Compactness: the curve can be parameterized very compactly by its control vertices V_i;
- Locality: only the corresponding portions of the curve need to be modified if certain control vertices are changed;
- Flexibility: corners and straight line segments of the curve can be imposed if appropriate control vertices are used; and

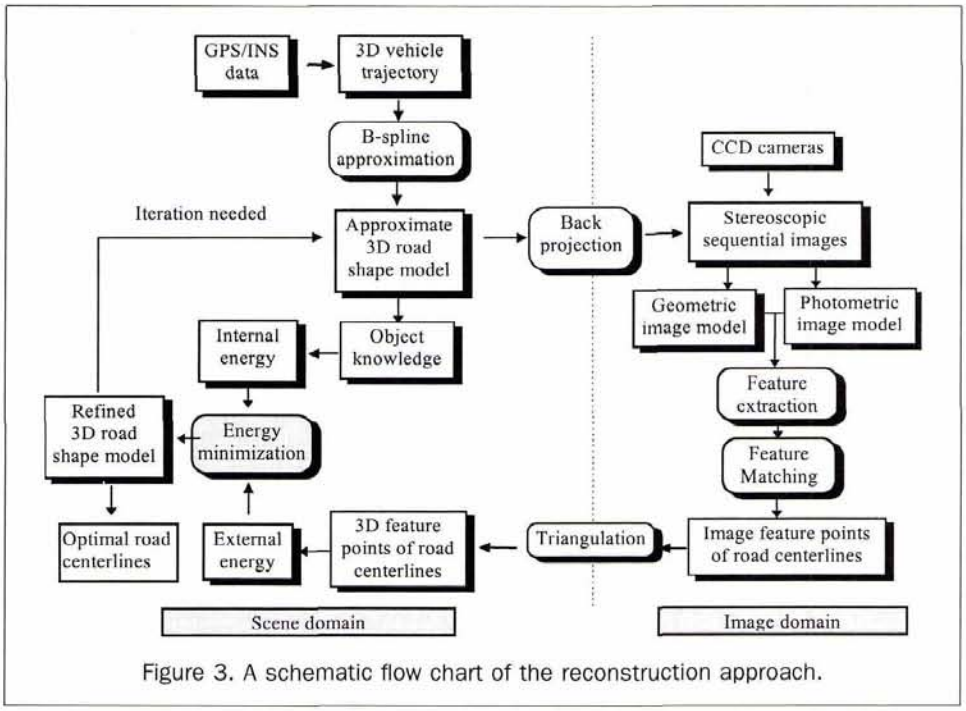

Figure 3. A schematic flow chart of the reconstruction approach.

- Invariance: the control vertices are invariant to affine and projective transformations (Cohen *et al.*, 1995).

Furthermore, the B-spline representation can be extended to a deformation curve model (B-snake), which is a key component of this research. Using vehicle trajectory data, the approximate centerline model is generated using a least-squares adjustment. The detailed mathematical description of B-spline approximation based on discrete data can be found in Bartels *et al.* (1987).

Extraction of Road Centerlines from Image Sequences

Highly accurate methods (El-Sheimy and Schwarz, 1993) have been developed to calibrate the mobile mapping system and to calculate parameters of geometric transformations between the vehicle coordinate system and various sensor systems, such as GPS, INS, and cameras. As a result, the image sequences are georeferenced in a global coordinate system. This makes the transformation from image-to-scene and scene-to-image possible.

A two-stage process is applied to extract road centerline information from the image sequences: extraction of feature points of the road centerlines and matching of the extracted feature points along the image sequences.

Model-Driven Feature Extraction

The approximate positions of the road centerlines on the images can be predicted by backward projection (scene-to-image transformation) of the approximate road model in the scene domain derived from the dynamic GPS observations. The feature extraction is performed within a constrained search window in the scene domain in order to reduce the searching range along the road. This searching is determined considering the vanishing line condition (Figure 4) and the lane width in the scene domain (Tao *et al.*, 1996). Features of the road centerline model are represented by two edges in the imagery. Taking the characteristics of terrestrial images and the system configuration into consideration, a set of rules are established to extract reliable features in the implementation (Table 1).

In mobile mapping images, the major index of centerline edges is edge-gradient orientation rather than gradient amplitude. The amplitude does not provide sufficient information for classifying an edge to be a centerline edge, because the edge may be affected by factors such as severe noise, shadows, road surface materials, and marking quality. However, the gradient of a centerline edge is almost perpendicular to the predicted centerline (Figure 4), and independent of its amplitude. Furthermore, as illustrated in Figure 5, if an edge is oriented at 45°, a non-oriented edge detector may find a gradual slope in the edge profile. On the other hand, an oriented edge detector defines a sharp edge and locates the edge more efficiently. Because the window size of edge detectors is limited, for example, 3 pixels by 3 pixels, actual gradients calculated by non-oriented and oriented edge detectors are also different. The latter usually supplies higher quality gradients.

Calculation of gradients of large image sequences is a very time consuming process. A great deal of time can be saved if this operation can be restricted to a set of specific image points. The oriented edge-detection algorithm is implemented with three steps. First, to avoid the gradient calculation at all image points, four directional *Prewitt* masks (Pratt, 1991) defining directions of north-south, northeast-southwest, east-west, and southeast-northwest are used to

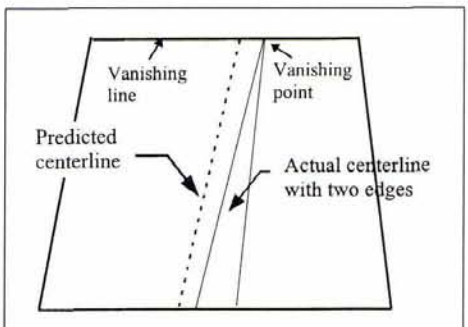

Figure 4. Predicted and actual road centerlines in the image domain.

TABLE 1. A SET OF RULES FOR CENTERLINE FEATURE EXTRACTION

Rule #	Rule Name	Rule Description
Rule 1	Amplitude	The amplitude of the edge should surpass a certain threshold.
Rule 2	Direction1	The direction of the edge should be parallel to the predicted centerline with a tolerance $\pm 20°$.
Rule 3	Direction2	The gradient directions of the two edges of a centerline must be opposite to each other with a tolerance of $\pm 15°$.
Rule 4	Distance	The distance between the two edges of a centerline should be within a few pixels (2-5 pixels).
Rule 5	Gray value	The average gray value within the centerline area must surpass a threshold and be brighter than its immediate lateral neighboring areas.
Rule 6	Continuity	Distances (defined in Rule 4) for adjacent segments should not be significantly different and the difference should be within a threshold.
Rule 7	Smoothness	The centerline should be a relatively smooth line.

convolute the images. At each point, responses of the four Prewitt masks are compared. The direction code whose corresponding response is maximum at the point is assigned to the point. According to Rule 1 in Table 1, image points with high gradient amplitudes are considered and a further edge thinning process (Nevatia and Babu, 1980) is applied. For this reduced set of edge points, the Sobel gradient operator that is oriented according to the direction codes is executed. Examining the calculated edge gradients, Rule 2 can be implemented. The number of remaining edges is thus greatly reduced.

Road centerlines are usually painted in white or yellow and are of a certain width. They appear as dual edges with one edge on each side of the line in the images. Consequently, a dual edge-detection algorithm is designed to refine the result of the candidate edges. Suppose that an edge is on one side of the actual centerline. A corresponding edge on the other side should exist. The gradient directions of the edges are opposite (Rule 3). The distance between them must satisfy Rule 4. In addition, the average gray value between them should surpass a threshold and be brighter than its immediate lateral neighboring areas (Rule 5). This process greatly eliminates undesired edges and results in detected dual edges as short line segments.

Rule 6 and 7 are implemented using a so-called majority voting method. An advantage of this method is that a distribution of majority dual edges along a smooth line can be determined. Meanwhile, blunders that are edges not on the line can be eliminated. Similar to a histogram, a parameter space is defined (Figure 6b), with the horizontal axis as the distance between the centroid of a dual edge and the predicted centerline, and the ordinate axis as the number of dual edges with the corresponding distance. Because the dual edges are preprocessed using Rules 1 to 5, those of the centerline represent the majority of all candidate edges. They should form a peak at point D_0, which is the average distance between the predicted and actual centerlines. Edges outside of the tolerable range of $D_0 \pm 1.5$ pixels are treated as blunders and eliminated.

Stereo-Matching Using Sequential Images

The potential centerline features extracted exist in individual images. They should be matched between stereoscopic image sequences to produce 3D feature points in the scene domain.

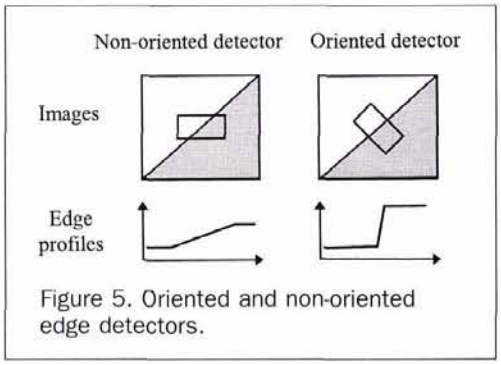

Figure 5. Oriented and non-oriented edge detectors.

The matching algorithm takes full advantages of the geometric strength of the mobile mapping data.

A key task in the matching process is to find corresponding centerline edges within a searching range. The reliability and efficiency of the algorithm greatly depend on the range defined. This range should be as small as possible, yet produce reliable results, implying that the corresponding edge must be inside this range. As illustrated in Figure 7a, a centerline point (marked as a cross) on image A is projected onto image B as the approximate location of its corresponding point. This is realized under two conditions: (1) exterior-orientation parameters are known (derived from GPS and INS data), and (2) the road surface is assumed to be a plane whose parameters are estimated from both the known camera height with respect to the ground and the vehicle frame orientation (Tao *et al.*, 1996). Along with the epipolar line (dotted lines in Figure 7a) constraint, the one-dimensional searching range on image B can be restricted to a relatively small area.

Although the searching range is reduced, mismatches or matching failures may sometimes occur because of the large difference between centerline orientations in the two image windows caused by camera-object geometry (Figure 7a). To overcome this difficulty, the two image windows are projected onto a plane that is parallel to the assumed ground plane by a plane-to-plane transformation (Figure 7b). Image features on the road surface after the transformation are

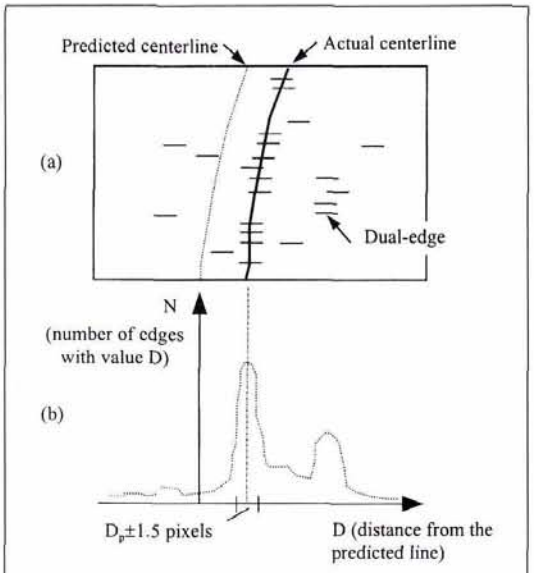

Figure 6. Majority voting method for identification of centerline edges.

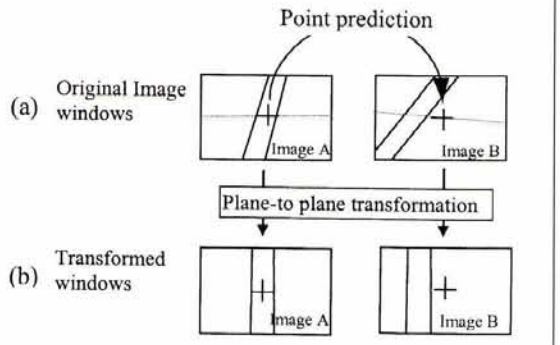

Figure 7. Ground-plane based distortion correction and matching.

much better suited for comparison. The matching process is performed using these transformed windows.

A centerline segment in the scene domain has usually several appearances in the image sequences, for example, images A_{Ti} and B_{Ti} taken at time epoch T_i, and A_{Ti+1} and B_{Ti+1}, taken at time epoch T_{i+1} (Figure 8). Three pairs of epipolar lines (dotted lines) can be calculated between the master image A_{Ti} and searching images B_{Ti}, A_{Ti+1}, and B_{Ti+1}. For a centerline point P_0 on the master image A_{Ti}, the SSD (sum of squared difference) algorithm (Kanade *et al.*, 1992), because of its simple structure and high performance, is applied to find corresponding points (marked with •) in the other three images, using the restricted searching ranges and transformed windows. The boxes along the epipolar lines in Figure 8 depict the searching ranges. To check the consistency of the multi-image matching result in image B_{Ti+1}, the corresponding points for the matched point P_3 of image A_{Ti+1} and P_1 of image B_{Ti} are found by the same matching algorithm and marked with △ and ×, respectively. Ideally, all three corresponding points marked with •, △, and × should be at the same point. In practice, if any two of them are close and the distance between them is smaller than 1.5 pixels, the corresponding image pair is chosen and the feature points are used to calculate the centerline points in the scene domain by a photogrammetric intersection. In the example of Figure 8, P_0 and P_3 may be considered as a matched point pair because in image B_{Ti+1} the distance between points △ and • is less than 1.5 pixels and it is the shortest one among all distance combinations of the three points. However, depending on the position of the point in the scene domain with respect to the baseline (A_{Ti} and A_{Ti+1}), an effective baseline that is much smaller in this case can also be used to reject this point pair because the short effective baseline may cause low 3D accuracies. P_0 and P_1 are checked using the same criteria and may be accepted. If no matched point pair is found, P_0 will be rejected. It should be noted that any image of the sequence with a feature point could be selected as a master image.

Refinement of 3D Road Centerlines by a Dynamic Physical Model

The points obtained by the aforementioned matching algorithm and photogrammetric intersections are 3D discrete points along the road centerline in the scene domain. A 3D model whose parameters are determined by the matched points then describes the centerline. The quality of these points can also be checked and improved by an iterative refinement procedure.

Deformation models have been researched and applied in edge detection, stereo matching, and object modeling (Kass *et al.*, 1988; Terzopoulos *et al.*, 1988; Fua, 1991; Pentland and Sclaroff, 1991; Trinder and Li, 1995; Gruen and Li, 1996). The main advantage of deformation models is that both geometric and physical constraints can be incorporated. In comparison, conventional models consider only geometric constraints. In this research, a 3D physical deformable curve model is employed to combine multiple information sources for reconstruction of the 3D road centerlines.

Physical Deformation Mechanism

The 3D parametric curve model described by the B-spline $Q(u)$ in Equation 1 can be treated as a deformable and elastic model, or a 3D B-snake (Menet *et al.*, 1990). Physically, it is assumed to be composed of an abstract material. The model evolves from its initial shape towards the desired one driven by external forces applied and internal forces generated. In accordance with the least-action principle, also called Hamilton's principle (Courant and Hilbert, 1953), the dynamics of the deformation model are described by

$$E = e_1 E_{int}(Q(u)) + e_2 E_{ext}(Q(u)) \rightarrow \text{minimum} \qquad (2)$$

where E_{ext} represents the external energy applied on the model, and E_{int} is the internal energy that resists the deformation from its natural state. e_1 and e_2 are constants for weighting the contributions of the two energy terms. The minimization of the total energy E of the motion equation governs the behavior of the deformation model.

E_{int} is further described as the smoothness energy consisting of two terms:

$$E_{int} = \alpha \left(\int_0^1 |Q'(u)|^2 \, du \right) + \beta \left(\int_0^1 |Q''(u)|^2 \, du \right). \qquad (3)$$

The first derivative $Q'(u)$ is a measure of the distance discontinuities (stretching effectiveness), while the second derivative $Q''(u)$ is a measure of the orientation discontinuities (bending effectiveness). Adjusting the weights α and β controls the relative balance of the stretching and bending forces. E_{int} is responsible for maintaining the local continuity and connectivity of the curve model. It also ensures that the curve will not be torn apart, fold onto itself, or exhibit a high curvature. In general, the internal energy controls the global shape of the model.

The external energy drives the model into the desired shape (Figure 9). The extracted 3D feature points P_i act as external forces and enforce the model $Q(u)$ to deform accordingly. In order to quantify the forces, a gravity-type field is

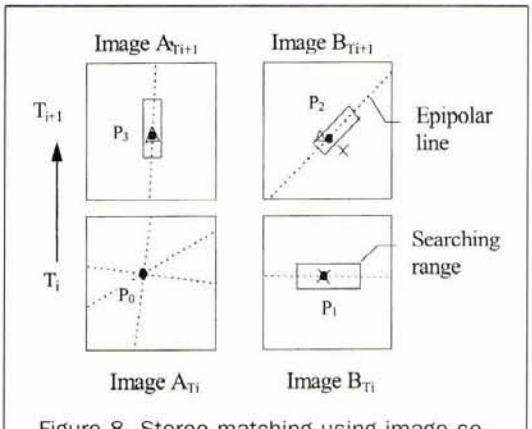

Figure 8. Stereo matching using image sequences.

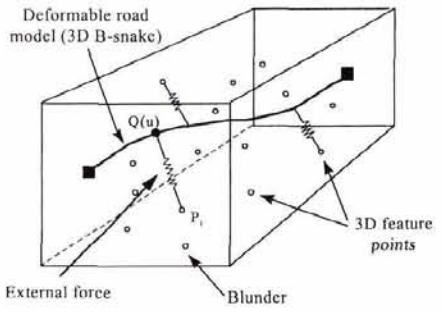

Figure 9. Deformation behavior of the model driven by the external energy.

used. Thus, the closer a feature point to the curve, the greater the force. The external energy is defined as

$$E_{ext} = f(x) = \begin{cases} x^2/2, & D_p < r_1 \\ 2 - x^{-1}, & r_1 \le D_p \le r_2 \\ 0, & D_p > r_2 \end{cases} \quad \text{and} \quad x = D_p/r_1, \tag{4}$$

where D_p is the distance between the curve $Q(u)$ and point P_i. r_1 and r_2 define the influence ranges of the feature points. They are chosen as $r_1 = 0.1$ (metre) and $r_2/r_1 = 4$. Within the range of $(0, r_2]$, the feature point is close to the curve and the function $f(x)$ acts like a spring. Points outside this range, $D_p > r_2$, do not have any influence on the model deformation. This characteristic practically eliminates or minimizes the effect of blunders because they are usually distant from the curve. In addition, the function prevents itself from being singular for points exactly along or very close to the curve. The corresponding external force can be derived from the external energy:

$$F_{ext} = \nabla E_{ext} = f'(x) = \begin{cases} x, & D_p < r_1 \\ x^{-2}, & r_1 \le D_p \le r_2 \\ 0, & D_p > r_2. \end{cases} \tag{5}$$

Considering the temporal effect of the external force during the period of $[T_{i-1}, T_{i+1}]$, the total force F_{ext} becomes

$$F_{ext} = \omega_1 F_{ext}(T_{i-1}) + \omega_2 F_{ext}(T_i) + \omega_3 F_{ext}(T_{i+1}) \tag{6}$$

where ω_1, ω_2, and ω_3 are weights.

Solution for Energy Minimization

Observing Equations 1, 3, and 5, the discrete version of the motion function in Equation 2 can be written as

$$E = \sum_{j=0}^{n-1} \{e_1[\alpha(u_j) (\sum_{i=0}^{m-1} V_i B_i'(u_j))^2 + \beta(u_j) (\sum_{i=0}^{m-1} V_i B_i''(u_j))^2 + e_2 F_{ext}[Q(u_j)]\}. \tag{7}$$

The total energy E is a function of the set of control vertices that influence the shape of the curve model. The minimization of the energy results in the final state of the control vertices.

The minimization of E in Equation 7 requires that

$$\partial E / \partial V_k = 0, \quad k = 0, 1, 2, \ldots, m. \tag{8}$$

The resultant equations can be derived and solved by using a Lagrangian dynamic motion equation. Implementation details of the minimization algorithm can be found in (Tao, 1996).

Results and Evaluation

Computational Considerations

A number of parameters must be set before the whole procedure can be started. A trade-off between the internal energy and external energy should be made in order to balance the global and local characteristics of the deformation model. Considering the configuration of the mobile mapping system used and the images acquired in this research, $e_1 = 0.3$ and $e_2 = 0.7$ $(= 1 - e_1)$ are applied in Equation 2. The smoothness coefficients in Equation 3 are empirically determined as $\alpha = 0.7$ and $\beta = 0.5$ to maintain the road shape. The weights in Equation 6 are chosen as $\omega_1 = 0.5$, $\omega_2 = 1.0$, and $\omega_3 = 0.8$.

Two major high computational demands are (1) feature point extraction and subsequent matching and (2) inversion of matrices involved in the minimization process. The constrained feature extraction method and the restricted searching window in the matching process greatly reduce the computational load. The inversion problem was solved by introducing a decomposition of the entire model into deformable model segments. The detailed description of the implementation of the algorithm can be found in Tao (1996).

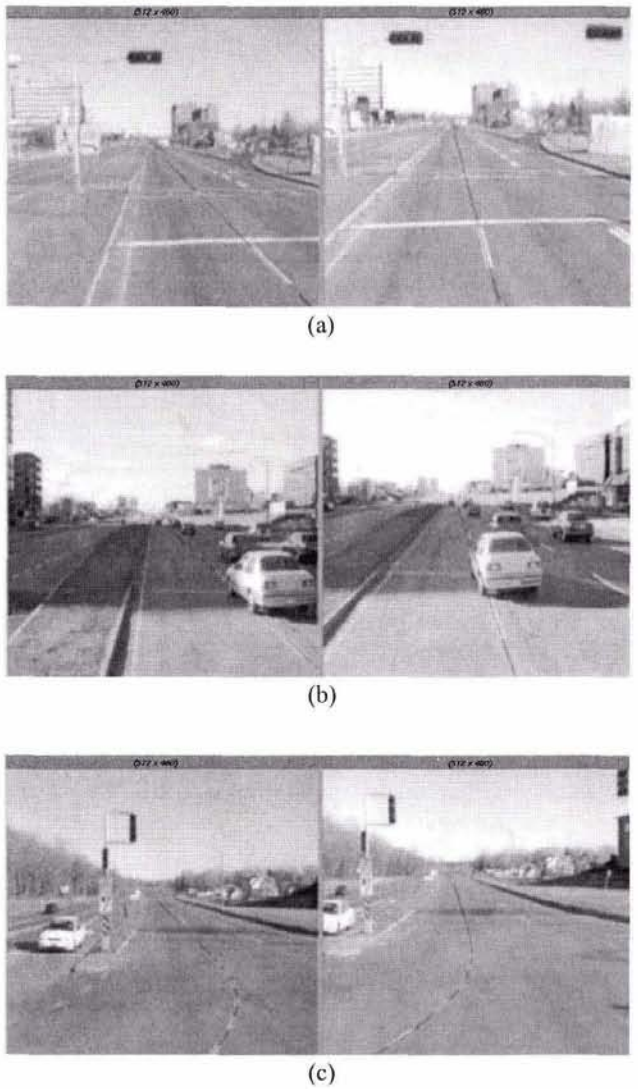

(a)

(b)

(c)

Figure 10. Road centerlines extracted in various situations described in Figure 1.

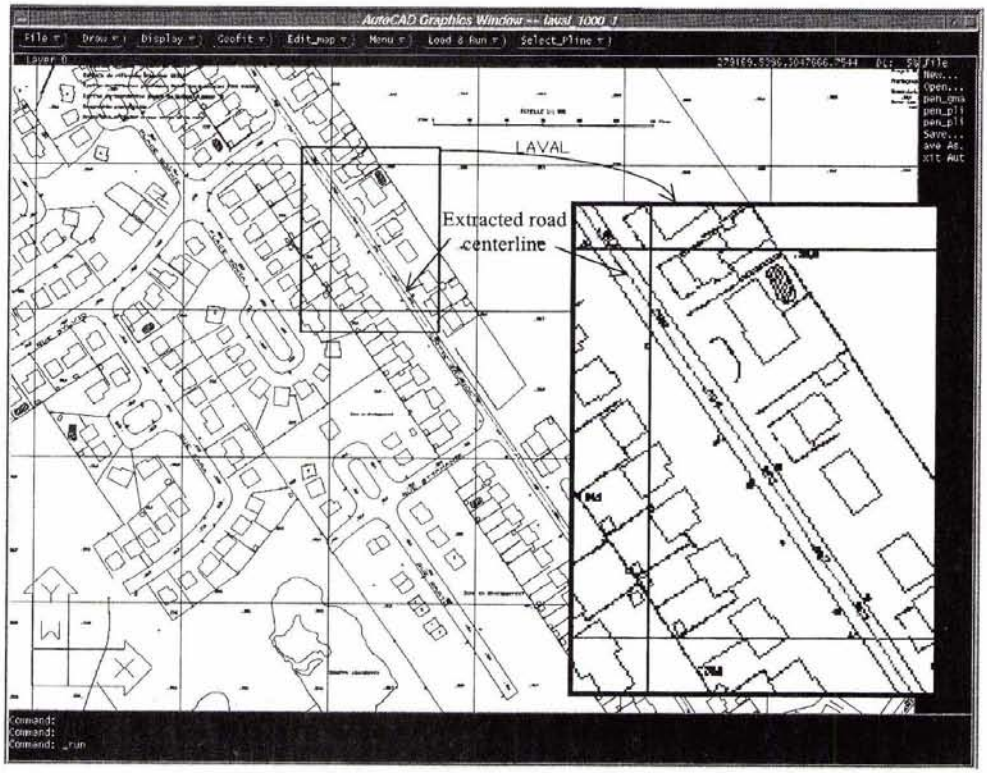

Figure 11. Extracted road centerlines overlaid on a digital map.

The software system based on this approach has been developed within an automatic mobile mapping data processing package called ImagExpert. The package is developed in a UNIX workstation environment. A high level object-oriented X-Window development toolkit, WNDX, was used to design the graphic user interface (GUI). The package has also an interface with AutoCAD for displaying processed and existing vector information. This built-in interface in the package creates an efficient environment for both automatic and interactive operations in image and scene domains (Li *et al.*, 1994).

Evaluation of the Test Results

The introduced approach has been tested using image sequences from two data sets. Data Set I and II were acquired in Laval and Quebec City, Quebec, respectively. The vehicle speed was 50 to 60 km per hour and the imaging rate was set as 0.4 second per image. Each data set contains several image sequences covering different areas of a city. At each exposure station, a pair of forward-looking stereo images and a right-looking image were taken. Data Set I was collected after 4:00 PM in winter and the lighting condition was relatively poor. The images covering streets in city of Laval have low brightness and low contrast. This causes some loss of image details. For examining the robustness of the approach, the data set was used without image preprocessing. Data Set II was taken mainly along highways of Quebec City during daytime. It has better image quality.

Before starting the automatic procedure of centerline extraction, it is required that the operator give two initial image points indicating the direction and approximate location of the centerline to be extracted. The rest of the procedure is fully automatic and can be executed in a batch mode. The resulting centerline segments in the scene domain can be back-projected onto the images, allowing one to monitor the processing progress and quality. It also allows the operator to interrupt the process and perform on-line corrections. Among the image sequences processed, the longest one is a highway image sequence of Data Set II in Quebec city, which contains 1665 images. Various difficult situations were dealt with by the approach. Figure 10 illustrates some examples of the centerlines successfully extracted (represented by black lines). The pedestrian crossing lines create a large gap along the lane separating line (Figure 10a). Furthermore, the shadow of a building changes the image contrast along the line and a moving car blocks a portion of the line (Figure 10b). The curved centerline at a T-intersection was extracted (Figure 10c). Figure 11 shows the overlay of the extracted and reconstructed centerlines on a digital map (1:1,000 map scale) of Laval. The coordinates of the centerlines in the WGS-84 reference system that was used for DGPS calculation were converted to those in the UTM system used by the digital map before performing the overlay. Note that the centerlines fit the map well.

The evaluation of the testing results is carried out in two steps. First, the extracted centerlines in the scene domain are back-projected onto images to check if the projections match the corresponding image edges. This provides a measure of the relative accuracy. Second, the absolute accuracy is checked by overlaying the extracted centerlines on the existing digital road maps in the map display environment of OverView (Li *et al.*, 1994). The implemented system was capable of dealing with scenes with various marking patterns, road classes, and difficult road conditions. It found blunders occurring in places where the vehicle approached big gaps or sharp turns. It was able to filter them out after new centerline segments beyond the places were extracted. A tolerance of 5 pixels was set, which matches the corresponding camera orientation errors. No differences between the back-projected

centerlines and the corresponding image edges exceeded the tolerance. A comparison with selected control points indicated that the positional accuracy of the centerlines could reach 30 cm.

Concluding Remarks

An integrated approach to automatic reconstruction of road centerlines from mobile mapping image sequences is introduced. The reconstruction problem is treated as an inverse problem and solved by global optimization techniques. This approach utilizes unique constraints that exist only in mobile mapping image sequences. The research results also make a contribution to the general field of *structure from motion and stereo*. Based on this research, the following conclusions can be drawn:

- The introduced approach uses a closely coupled bottom-up and top-down centerline reconstruction scheme. The reconstruction process is designed based on a 3D shape model and image sequences. This leads to a robust result because both local and global shapes are controlled by the adjustment of the combined internal energy (model) and external energy (images).
- The synthesis of multiple constraints was implemented by the least-action principle. One of its advantages is that the constraints from both the model assumptions and the image sequences can be incorporated into a mathematical model. The model with the combined constraints can be solved by using a Lagrangian motion equation.
- The information derived from multiple sensors, such as GPS and INS, provides not only the camera orientation parameters, but also other significant information and constraints, such as the approximate 3D centerline model and the road surface plane.
- The centerline image edges are modeled by a set of rules. Guided by the rules, a hierarchical edge-detection algorithm, including oriented edge detection, dual-edge detection, and edge filtering, is developed. The majority voting method effectively determines image centerline edges by using information from the scene domain.
- A robust matching method is achieved by integration of constraints derived from the navigation data and image sequences, such as the multiple epipolar line constraint, ground plane constraint, and temporal image sequence constraint.
- Both geometric characteristics and numeric advantages of the B-Spline based 3D snake representation are utilized for improving the system efficiency. It is particularly significant in reduction of unknown numbers in the piece-wise solution of the minimization problem.

Acknowledgments

Collaboration with Dr. K.P. Schwarz has been very valuable. Research support from the Natural Sciences and Engineering Research Council (NSERC) of Canada and GEOFIT Inc., Laval, Quebec is gratefully appreciated. Reviewers and editor's comments are appreciated.

References

Bartels, R., J. Beatty, and B. Barsky, 1987. *An Introduction to Splines for Use in Computer Graphics and Geometric Modeling*, Morgan Kaufmann.

Cohen, F.S., Z. Huang, and Z. Yang, 1995. Invariant Matching and Identification of Curves Using B-Splines Curve Representation, *IEEE Trans. on Image Processing*, 4(1):1–10.

Courant, R., and D. Hilbert, 1953. *Methods of Mathematical Physics*, Vol.I, Interscience, London.

Dickmann, E.D., and A. Zapp, 1986. A Curvature-Based Scheme for Improving Road Vehicle Guidance by Computer Vision, *Mobile Robots*, Cambridge, Massachusetts, SPIE, 727:161–168.

Dickinson, S., and L. Davis, 1990. A Flexible Tool for Prototyping AVL Road Following Algorithms, *IEEE Trans. on Robotics and Automation*, 6(2):232–242.

El-Sheimy, N., and K.P. Schwarz, 1993. Kinematic Positioning in Three Dimensions Using CCD Technology, *Proceedings of IEEE - Vehicle Navigation and Information System Conference (IVHS)*, pp. 472–475.

Fua, P., 1991. Combining Stereo and Monocular Information to Compute Dense Depth Maps that Preserve Depth Discontinuities, *Proceedings of the 12th International Joint Conference on Artificial Intelligence*, Sydney, Australia, pp. 1292–1298.

Geiselmann, C., and M. Hahn, 1994a. Identification of Simple Objects in Image Sequences, *International Archives of ISPRS*, 30(Part B3/1):288–1295.

———, 1994b. Identification and Location of Simple Objects for Real-time Mapping, *International Archives of ISPRS*, 30(Part 2): 459–470.

Gruen, A., and H. Li, 1996. Linear Feature Extraction with LSB-Snakes from Multiple Images, *International Archives of ISPRS*, 31(Part B3):266–272.

He, G., and K. Novak, 1992. Automatic Analysis of Highway Features from Digital Stereo Images, *International Archives of ISPRS*, 29(Part B3):119–124.

Jolion, J.-M., 1994. Computer Vision Methodologies, *CVGIP: Image Understanding*, 59(1):53–71.

Kanade, T., M. Okutomi, and T. Nakahara, 1992. A Multiple-Baseline Stereo Method, *Proceedings of ARPRA Image Understanding Workshop*, San Diego, California, pp. 409–426.

Kass, M., A. Witkin, and D. Terzopoulos, 1988. Snakes: Active Contour Models, International Journal of Computer Vision, 1(4):321–331.

Li, R., K.P. Schwarz, M.A. Chapman, and M. Gravel, 1994. Integrated GPS and Related Technologies for Rapid Data Acquisition, *GIS World*, 7(4):41–43.

Menet, S., P. Saint-Marc, and G. Medioni, 1990. Active Contour Models: Overview, Implementation and Applications, *International Conference of Systems, Man and Cybernet*, Los Angeles, pp. 194–199.

Nevatia, R., and K.R. Babu, 1980. Linear Feature Extraction and Description, *Computer Graphics and Image Processing*, 13(2):257–269.

Pentland, A., and S. Sclaroff, 1991. Closed-Form Solution for Physically Based Shape Modeling and Recognition, *IEEE Trans. on Pattern Analysis and Machine Intelligence*, PAMI-13(7):715–729.

Pratt, W.K., 1991. *Digital Image Processing*, John Wiley & Sons, Inc.

Schneiderman, H., and M. Nashman, 1994. A Discriminating Feature Tracker for Vision-Based Autonomous Driving, *IEEE Trans. on Robotics and Automation*, 10(6):769–775.

Schwarz, K.P., H. Martell, N. El-Sheimy, R. Li, M. Chapman, and D. Cosandier, 1993. VISAT - A Mobile Highway Survey System of High Accuracy, *Proceedings of IEEE - Vehicle Navigation and Information System Conference (IVHS)*, pp. 476–481.

Tao, C., 1996. Road Centerline Reconstruction from Sequential Images Based on Shape from Sequences, *SPIE Proceedings of Visual Communication and Image Processing*, Orlando, Florida, SPIE, 2727:1251–1262.

Tao, C., R. Li, and M.A. Chapman, 1996. Model Driven Extraction of Road Line Features Using Stereo-Motion Constraints from a Mobile Mapping System, *Proceedings of ASPRS/ACSM Annual Convention*, 2:135–144.

Terzopoulos, D., A. Witkin, and M. Kass, 1988. Constraints on Deformable Models: Recovering 3D Shape and Non-Rigid Motion, *Artificial Intelligence*, 36(1):91–123.

Thorpe, C., M. Hebert, T. Kanade, and S. Shafer, 1988. Vision and Navigation for the Carnegie-Mellon Navlab, *IEEE Trans. on Pattern Analysis and Machine Intelligence*, 10(3):362–372.

Trinder, J.C., and H. Li, 1995. Semi-Automatic Feature Extraction by Snakes, *Automatic Feature Extraction of Man-made Objects from Aerial and Space Images* (A. Gruen, O. Kuebler, and P. Agouris, editors), Birkhaeuser Verlag, Basel.

———, 1996. Extraction of Man-Made Features by 3-D Active Contour Models, *International Archives of ISPRS*, 31(Part B3):874–879.

(Received November 1996; revised and accepted 23 December 1997)